

Self-consistent multidimensional Penrose process driven by magnetic reconnection

FILIPPO CAMILLONI¹ AND LUCIANO REZZOLLA^{1,2,3}

¹*Institut für Theoretische Physik, Goethe Universität, Max-von-Laue-Straße 1, 60438 Frankfurt am Main, Germany*

²*School of Mathematics, Trinity College, Dublin 2, Ireland*

³*Frankfurt Institute for Advanced Studies, Ruth-Moufang-Str. 1, 60438 Frankfurt am Main, Germany*

(Dated: March 24, 2025)

ABSTRACT

Astronomical observations and numerical simulations are providing increasing evidence that resistive effects in plasmas around black holes play an important role in determining the phenomenology observed from these objects. In this spirit, we present a general approach to the study of a Penrose process driven by plasmoids that are produced at reconnection sites along current sheets. Our formalism is meant to determine the physical conditions that make a plasmoid-driven Penrose process energetically viable and can be applied to scenarios that are matter- or magnetic-field-dominated, that is, in magnetohydrodynamical or force-free descriptions. By exploring reconnection from an axisymmetric but curved surface, our approach can be considered genuinely multidimensional and allows us to explore conditions that are beyond the ones explored so far and that have been restricted to the equatorial plane. Furthermore, it provides a direct contact with numerical simulations of accretion onto black holes, which exhibit an intense reconnection activity outside the equatorial plane. Finally, to describe the kinematics of the plasma self-consistently, we use the well-known configuration of an equilibrium torus with a purely toroidal magnetic field. For such a torus, we discuss the existence of an “ergobelt”, i.e., a nontrivial surface penetrating the ergosphere and acting as a natural site for the occurrence of reconnection, and from where we estimate the energetics of a plasmoid-driven Penrose process.

1. INTRODUCTION

In a resistive plasma, magnetic reconnection consists in a sudden rearrangement of the magnetic-field topology caused by the local interaction of field lines with opposite polarity. This process leads to a rapid conversion of magnetic energy into thermal and kinetic energy of two plasma outflows with locally isotropic properties and moving in opposite directions at relativistic speeds, the plasmoids. The ubiquitous and fundamental role played by magnetic reconnection in astrophysical plasmas is now widely recognized on scales ranging from stellar flares and coronal mass ejections (Su et al. 2013; Zweibel & Yamada 2009; Yamada et al. 2010), to high-energy sources such as pulsar magnetospheres (Uzdensky & Spitkovsky 2013), accreting black holes (BHs) (Beloborodov 2017; Ripperda et al. 2019; Akiyama & et al. 2019; Event Horizon Telescope Collaboration et al. 2022), and binary neutron-star mergers leading to the short gamma-ray burst phenomenology (Palenzuela et al. 2009; Liu et al. 2008; Anderson et al. 2008; Rezzolla et al. 2011; Palenzuela et al. 2013; Kiuchi et al. 2015; Dionysopoulou et al. 2015).

Recent analytic studies, as well as numerical simulations, either in magnetohydrodynamics (MHD) or with particle-in-cell (PIC) approaches, have unfolded a rich phenomenology associated to magnetic reconnection and plasmoid genera-

tion, thus enhancing our understanding of these processes both in special-relativistic regimes (Liu et al. 2017; Comisso & Asenjo 2014; Guo et al. 2014; Asenjo & Comisso 2015; Liu et al. 2015; Ball et al. 2018; Meringolo et al. 2023), and when general-relativistic effects become relevant (Koide & Arai 2008; Asenjo & Comisso 2017; Parfrey et al. 2019; Comisso & Asenjo 2021; Bransgrove et al. 2021; Fan et al. 2024; Shen & YuChih 2024). In this regard, astrophysical BHs constitute unique theoretical laboratories to explore extreme conditions of plasma electrodynamics. Indeed, one the most remarkable predictions of general relativity is the possibility of extracting rotational energy of the BH by invoking the negative inflow of energy and angular momentum at the horizon (Lasota et al. 2014), with various processes differing only in the physical agent operating the extraction. Notable examples range from single particles associated to mechanical (Penrose & Floyd 1971; Ruffini et al. 2024) and collisional Penrose process (PP) (Bañados et al. 2009; Bejger et al. 2012; Schnittman 2014; Berti et al. 2015), to super-radiant scalar fields (Press & Teukolsky 1972; Pani et al. 2012; Bosch et al. 2016; East & Pretorius 2017), and to force-free electrodynamics (FFE) fields in the Blandford–Znajek (BZ) mechanism (Blandford & Znajek 1977; Dadhich et al. 2018).

Given the presence of strong magnetic fields and relativistic plasmas near astrophysical BHs, it is natural to expect a manifestation of the PP triggered by magnetic reconnection and mediated by plasmoids. This idea was originally proposed and explored analytically by Koide and Arai (Koide & Arai 2008), to be further reviewed and extended by Asenjo and Comisso (Asenjo & Comisso 2017; Comisso & Asenjo 2021), who computed the power extracted and the efficiency of the process in terms of the local reconnection rate (see also Parfrey et al. 2019, for related PIC simulations). The basic picture of this process involves a current-sheet with large aspect-ratio forming within the BH ergosphere. As ordinary in reconnection processes, such a current-sheet fragments via the tearing instability into a chain of plasmoids (or magnetic flux-tubes in three dimensions) that are accelerated away from the reconnection layer, becoming an efficient channel to transport magnetic energy away from the reconnection site. In a steady state, pairs of plasmoids are ejected from the reconnection site, where, for each pair, a plasmoid will move outwards to large distances, while the other one will be ingoing and move towards the event horizon. If the ingoing plasmoid has a negative energy-at-infinity, it will drive a PP. It is important to note that the plasmoid that is relevant for the PP is the ingoing one and that it needs to travel only a lengthscale of $\mathcal{O}(M)$ within the ergosphere to reach the event horizon and extract energy via the PP. The details of what happens to the outgoing plasmoid are not important for the success of the PP, and the outgoing plasmoid could transmit its energy-at-infinity just outside the ergosphere after being converted into electromagnetic bursts or at very large distances (e.g., via synchrotron cooling¹). The PP would work in either case.

Despite the importance of the initial works by Koide & Arai (2008) and Comisso & Asenjo (2021), they contain a number of approximations that prevent from testing them in numerical environments and assessing their viability in realistic astrophysical scenarios. Arguably, the most serious of these limitations rests with the lack of a self-consistent description of the plasma dynamics, either in the MHD or FFE regimes. In turn, this forces the use of number of assumptions on the dynamics of the plasma that are either far from known solutions and numerical simulations (see, e.g., Mahlmann et al. (2020); Ripperda et al. (2020); Nathanail et al. (2020, 2021); Ripperda et al. (2022); Crinquand et al. (2022); Dimitropoulos et al. (2024)), or difficult to realise in practice.

¹ Radiative losses are important in a realistic description of plasmoids propagating in the surrounding plasma and we expect these losses to be particularly relevant for those plasmoids travelling large distances of $\mathcal{O}(100 M)$ (Aimar et al. 2023) and for which synchrotron cooling can be effective. Radiative losses will instead affect only mildly those plasmoids that propagate from within the ergoregion to the event horizon, as they travel much shorter lengths of $\mathcal{O}(M)$.

To overcome these difficulties, it is important to construct reconnection models that are consistent with well-known plasma solutions or that share dynamical features and conditions that are similar to those encountered in simulations. The goal of this work is therefore that of having an analytic understanding of the energetics of the PP mediated by plasmoid for a non-trivial distribution of matter and electromagnetic fields. We do this by exploiting a self-consistent, fully covariant analytic description of plasma and fields of degenerate electrodynamicity that includes ideal MHD and FFE as particular examples. More specifically, we analyse for the first time the conditions under which a distribution of magnetised matter penetrating the ergosphere and not restricted to the equatorial plane can produce plasmoids with negative energy-at-infinity. In this way, we can study the extraction of energy and angular momentum from a Kerr BH in a self-consistent scenario that is not too far from the conditions explored in simulations. The ultimate expectation is that the insight that will be gained via these analytical calculations will be of help in understanding the results of the simulations of the plasmoid-driven PP once they will have reached a sufficient degree of realism.

2. DEGENERATE ELECTRODYNAMICS AROUND A KERR BH

We consider the electrodynamicity of a Kerr BH with mass M and specific angular momentum a . Following Thorne & Macdonald (1982), and introducing \mathbf{F} and $\eta_{\mu\nu\rho\sigma}$ respectively as the Faraday tensor and the Levi-Civita symbol, we refer to as *degenerate* those electromagnetic fields that satisfy the condition $\eta_{\mu\nu\rho\sigma} F^{\mu\nu} F^{\rho\sigma} = 0$ (or, equivalently, satisfying the condition of orthogonality between the electric and magnetic fields $\mathbf{E} \cdot \mathbf{B} = 0$) and *magnetically dominated* if i.e., $F_{\mu\nu} F^{\mu\nu} > 0$ (or, equivalently, if $B^2 - E^2 > 0$). Under this definition, force-free electromagnetic fields are clearly degenerate, but degeneracy can occur more generally and, indeed, an electromagnetic field can be degenerate without being force-free. This is because degeneracy appears whenever the electric field in the rest frame of the plasma vanishes, i.e., when $\mathbf{F} \cdot \mathbf{u} = 0$, where \mathbf{u} is the plasma four-velocity. Clearly, a plasma with infinite conductivity, such as that characterising the ideal-MHD limit, will have a zero comoving electric field and hence will be degenerate but not force-free. As a result, the conditions of a degenerate and magnetically dominated plasma describe both the force-free and the ideal-MHD conditions (see also Gralla & Jacobson 2014; Chael et al. 2023; Mizuno & Rezzolla 2024, for more recent discussions). The orthogonality of electric and magnetic fields and are violated only on the microscopical scales of the current-sheets where reconnection takes place (Liu et al. 2017). Degeneracy also implies that stationary and axisymmetric fields are expressed in terms of a magnetic-flux

function $\Psi = \Psi(r, \theta)$ that, under a suitable gauge choice, coincides with the toroidal component of the electromagnetic potential. As a result, constant- Ψ surfaces determine the poloidal magnetic fields, the poloidal current $I = I(r, \theta)$, which is proportional to the toroidal field, and the angular velocity of the magnetic-field lines $\Omega = \Omega(\Psi)$ (Gralla & Jacobson 2014).²

2.1. Zero angular momentum observer frame

A 3+1 decomposition of spacetime has a long history in BH electrodynamics (Landau & Lifshitz 2004; Thorne & Macdonald 1982), since it provides equations in a form that closely resembles the classical Maxwell equations, and can then be employed in numerical simulations. In this case, the metric can be written in terms the lapse function α , the shift vector β^ϕ and the spatial metric γ_{ij} (see Rezzolla & Zanotti 2013, and also the Appendix). Within this decomposition, a particularly convenient class of observers with a long history of use in the literature (Bardeen et al. 1972) is that with Zero Angular Momentum (ZAMOs) with worldline tangent

$$\eta := \eta^\mu \partial_\mu = \alpha^{-1}(\partial_t + \omega_z \partial_\phi), \quad (1)$$

and whose angular velocity is $\omega_z := -\beta^\phi$. Such an observer carries a local orthonormal (Cartesian) tetrad, $\hat{e}_{(\alpha)}$ with $\alpha = T, X, Y, Z$, such that on the equatorial plane ($\theta = \pi/2$), the X and Y legs align respectively with the r and ϕ directions, whereas the Z leg is orthogonal to the equatorial plane and parallel to the BH spin (quantities in the ZAMO frame are marked with a “hat” and the components with bracketed indices).

Introducing *F as the dual of the Faraday tensor, the magnetic field measured by the ZAMO, $\hat{B}^\mu := -{}^*F^{\mu\nu}\eta_\nu$, is purely spacelike, and in ZAMO-adapted coordinates one has that $\hat{\mathcal{B}} = \hat{B}^{(\alpha)}\hat{e}_{(\alpha)}$ reads

$$\hat{\mathcal{B}} = \frac{\partial_\theta \Psi}{\sqrt{\Pi} \sin \theta} \hat{e}_{(X)} - \frac{I}{\sqrt{\Delta} \sin \theta} \hat{e}_{(Y)} + \frac{\sqrt{\Delta} \partial_r \Psi}{\sqrt{\Pi} \sin \theta} \hat{e}_{(Z)}, \quad (2)$$

where

$$\Delta := r^2 - 2Mr + a^2, \quad (3)$$

$$\Pi := (r^2 + a^2)^2 - a^2 \Delta \sin^2 \theta, \quad (4)$$

are two metric functions of the Kerr solution and with the positions of the event horizons r_\pm given by roots of $\Delta = (r - r_+)(r - r_-)$ (see also the Appendix).

² Despite retaining axisymmetry as a working assumption, our approach is multidimensional, as the current-sheets associated with such configurations are off-equatorial and described by surfaces extending in the polar, azimuthal, and radial direction. This is in contrast with the equatorial current-sheets that only span the latter two.

The electric field, $\hat{\mathcal{E}}^\mu := F^{\mu\nu}\eta_\nu$, is orthogonal to $\hat{\mathcal{B}}$ and in the ZAMO basis $\hat{\mathcal{E}} = \hat{\mathcal{E}}^{(\alpha)}\hat{e}_{(\alpha)}$ reads

$$\hat{\mathcal{E}} = \frac{\sqrt{\gamma_{\phi\phi}}}{\alpha} (\omega_z - \Omega) (\hat{B}^{(Z)} \hat{e}_{(X)} - \hat{B}^{(X)} \hat{e}_{(Z)}), \quad (5)$$

so that it is possible to interpret $\hat{v}_F = \sqrt{\gamma_{\phi\phi}}/\alpha(\Omega - \omega_z)\hat{e}_{(Y)}$ as the field lines velocity in the ZAMO frame, and recover the usual expression $\hat{\mathcal{E}} = -\hat{v}_F \times \hat{\mathcal{B}}$.

The orthogonality of the electric and magnetic fields to each other and to the ZAMO four-velocity implies the following set of orthonormal vectors (McKinney 2006; Chael et al. 2023)

$$\begin{aligned} \mathcal{T}^{(\alpha)} &:= \eta^{(\alpha)}, & \mathcal{X}^{(\alpha)} &:= \frac{\hat{\mathcal{E}}^{(\alpha)}}{\sqrt{\mathcal{E}^2}}, & \mathcal{Y}^{(\alpha)} &:= \frac{\hat{B}^{(\alpha)}}{\sqrt{\mathcal{B}^2}}, \\ \mathcal{Z}^{(\alpha)} &:= \epsilon^{(\alpha)(\beta)(\gamma)(\delta)} \mathcal{T}_{(\beta)} \mathcal{X}_{(\gamma)} \mathcal{Y}_{(\delta)}. \end{aligned} \quad (6)$$

The plasma four-velocity as measured by a ZAMO, $\hat{u} = \hat{u}^{(\alpha)}\hat{e}_{(\alpha)}$ admits the generic decomposition in terms of components which are parallel, \parallel , or orthogonal, \perp , with respect to the magnetic-field lines (Komissarov 2004; McKinney 2006; Chael et al. 2023; Gelles et al. 2024)

$$\hat{u} = \hat{\gamma}(\mathcal{T} + \hat{v}_{\parallel} \mathcal{Y} + \hat{v}_{\perp} \mathcal{Z}). \quad (7)$$

Such a decomposition has the advantage that the spatial velocity orthogonal to the fields is solely specified by the electromagnetic sector, $\hat{v}_{\perp} := \mathcal{E}/\mathcal{B}$, and the corresponding Lorentz factor is $\hat{\gamma}_{\perp} := \sqrt{\mathcal{B}^2/(\mathcal{B}^2 - \mathcal{E}^2)}$, where $\mathcal{B}^2 - \mathcal{E}^2 > 0$. The total Lorentz factor $\hat{\gamma}$ is given by

$$\hat{\gamma} := \frac{1}{\sqrt{1 - \hat{v}_{\perp}^2 - \hat{v}_{\parallel}^2}}, \quad (8)$$

and we note that flows with $\hat{\gamma} = \hat{\gamma}_{\perp}$ (i.e., with $\hat{v}_{\parallel} = 0$) provide a unique covariant definition of timelike observers in FFE characterised by $\vec{E} \times \vec{B}$ drift velocities (McKinney 2006). Since the total Lorentz factor can also be expressed as $\hat{\gamma}^2 = \hat{\gamma}_{\perp}^2/(1 - \hat{\gamma}_{\perp}^2 \hat{v}_{\parallel}^2)$, it follows that $\hat{\gamma} \geq \hat{\gamma}_{\perp}$, namely, $\hat{\gamma} = \hat{\gamma}_{\perp}$ for $\hat{v}_{\parallel} = 0 =: \hat{v}_{\parallel}^{\min}$, and $\hat{\gamma} \rightarrow \infty$ for $\hat{v}_{\parallel} = \hat{\gamma}_{\perp}^{-1} =: \hat{v}_{\parallel}^{\max}$ (Chael et al. 2023).

2.2. Comoving frame

Because reconnection is normally studied locally, i.e., in the frame comoving with the plasma (Liu et al. 2017), we introduce the comoving frame with timelike tangent given by the plasma four-velocity \hat{u} . In the ideal-MHD limit of infinite electrical conductivity, any electric field is zero in the frame comoving with the fluid, so that if we define the electric, e , and magnetic, b , fields in the comoving frame respectively as $e^\mu := F^{\mu\nu}u_\nu$ and $b^\mu := -{}^*F^{\mu\nu}u_\nu$, then $e^\mu = 0$ by construction. Note that while we will employ a comoving

frame to compute the details of the reconnection and plasmoid production, we will always make use of the electromagnetic fields in the ZAMO frame, $\hat{\mathcal{E}}$ and $\hat{\mathcal{B}}$, so that the comoving magnetic field is

$$\mathbf{b} := \frac{\hat{\mathcal{B}} + (\hat{\mathbf{u}} \cdot \hat{\mathcal{B}})\hat{\mathbf{u}}}{\hat{\gamma}}, \quad (9)$$

and $b^2 := \mathbf{b} \cdot \mathbf{b} = \mathcal{B}^2 - \mathcal{E}^2$.

In the frame comoving with the fluid, we assume that two plasmoids are ejected locally tangent to the current-sheet with opposite ‘‘outflow’’ velocities $\pm \tilde{v}_{\text{out}}$, where the signs distinguish the plasmoid ejected in the direction parallel (+) or antiparallel (−) to the comoving magnetic-field lines as seen from one side of the reconnection layer³. The initial outflow four-velocity of the plasmoids is thus

$$\tilde{\mathbf{u}}_{\text{out}} = \tilde{\gamma}_{\text{out}}(\hat{\mathbf{u}} \pm \tilde{v}_{\text{out}} \mathbf{b}/b), \quad (10)$$

with the azimuthal velocity and Lorentz factor measured by the ZAMO given by

$$\hat{v}_{\text{out}}^{(Y)} = \frac{(\hat{\gamma}_{\perp} \hat{v}_{\parallel} \pm \tilde{v}_{\text{out}})\hat{\mathcal{B}}^{(Y)}}{\hat{\gamma}_{\perp}(1 \pm \hat{\gamma}_{\perp} \hat{v}_{\parallel} \tilde{v}_{\text{out}})\mathcal{B}} - \hat{v}_{\perp} \frac{\sqrt{\hat{\mathcal{B}}_{(X)}^2 + \hat{\mathcal{B}}_{(Z)}^2}}{\mathcal{B}}, \quad (11)$$

$$\hat{\gamma}_{\text{out}} = \hat{\gamma} \tilde{\gamma}_{\text{out}} (1 \pm \hat{\gamma}_{\perp} \hat{v}_{\parallel} \tilde{v}_{\text{out}}). \quad (12)$$

2.3. Plasmoids, RAIBs, and PP

To define the details of the PP we need a local model for magnetic reconnection that provides a prescription for the velocity field \tilde{v}_{out} of the plasmoids and their energetics. Such a model will have to account for the redistribution of the magnetic energy into the kinetic and internal energy of the plasmoid. The details of this conversion, which we here assume to originate from a hydrogen plasma, can be extremely

difficult to calculate under realistic conditions, and probably require a microscopical description involving PIC simulations (Ball et al. 2018; Meringolo et al. 2023). However, the most important reconnection quantities that we consider here, namely, the outflow velocity and the reconnection rate, emerge from MHD constraints and, as argued by Liu et al. (2017), are not sensitive on the microphysics as far as reconnection is mediated by plasmoids and the upstream plasma is in the collisionless regime (Comisso & Asenjo 2021). Approximate expressions for these quantities are given by

$$\tilde{v}_{\text{out}} \approx \sqrt{\sigma_0/(1 + \sigma_0)}, \quad \mathcal{R}_{\text{rec}} \simeq 0.1, \quad (13)$$

with σ_0 being the upstream plasma magnetisation.

Moreover, to make some analytic progress, we use the so-called Relativistic Adiabatic Incompressible Ball (RAIB) model (Koide & Arai 2008), normally adopted under these conditions (see Asenjo & Comisso 2017; Comisso & Asenjo 2021, and related works). Notwithstanding some of their limitations, RAIBs represent the simplest but non-trivial model of plasmoids, which are treated as localised distributions of energy dressed with an additional pressure term that contributes to their inertia and is reminiscent of their hydrodynamical nature. The RAIB energy-at-infinity needed to estimate the extraction of energy from a reconnection-driven PP follows upon integrating the energy-momentum tensor of a perfect fluid and reads (see Koide & Arai 2008, and also the Appendix)

$$E^{\infty} = \alpha H \left[\hat{\gamma}_{\text{out}} \left(1 + \frac{\sqrt{\gamma_{\phi\phi}}}{\alpha} \omega_z \hat{v}_{\text{out}}^{(Y)} \right) - \frac{U(\Gamma - 1)}{H \hat{\gamma}_{\text{out}}} \right], \quad (14)$$

with H , U , and Γ the total enthalpy, internal energy and adiabatic index in the plasmoid, respectively.

Hence, the energy-at-infinity per unit enthalpy, $\varepsilon^{\infty} := E^{\infty}/H$, is

$$\begin{aligned} \varepsilon_{\pm}^{\infty} = \alpha \hat{\gamma} & \left[\left(1 + \left(\hat{v}_{\parallel} \frac{\hat{\mathcal{B}}^{(Y)}}{\mathcal{B}} - \hat{v}_{\perp} \frac{\sqrt{\hat{\mathcal{B}}_{(X)}^2 + \hat{\mathcal{B}}_{(Z)}^2}}{\mathcal{B}} \right) \frac{\sqrt{\gamma_{\phi\phi}}}{\alpha} \omega_z \right) \tilde{\gamma}_{\text{out}} + \right. \\ & \left. \pm \left(\hat{v}_{\parallel} \hat{\gamma}_{\perp} + \left(\frac{\hat{\mathcal{B}}^{(Y)}}{\hat{\gamma}_{\perp} \mathcal{B}} - \hat{v}_{\parallel} \hat{v}_{\perp} \hat{\gamma}_{\perp} \frac{\sqrt{\hat{\mathcal{B}}_{(X)}^2 + \hat{\mathcal{B}}_{(Z)}^2}}{\mathcal{B}} \right) \frac{\sqrt{\gamma_{\phi\phi}}}{\alpha} \omega_z \right) \tilde{v}_{\text{out}} \tilde{\gamma}_{\text{out}} - \frac{U(\Gamma - 1)/H}{\hat{\gamma}^2 \tilde{\gamma}_{\text{out}} (1 \pm \hat{\gamma}_{\perp} \hat{v}_{\parallel} \tilde{v}_{\text{out}})} \right]. \end{aligned} \quad (15)$$

³ Under realistic conditions as those exhibited by the numerical simulations, plasmoids of different sizes and velocities are expected to be produced, so that \tilde{v}_{out} will actually follow a distribution (Huang & Bhattacharjee 2012).

Expression (15) contains information not only on the background geometry via the metric functions α , ω_z , and $\gamma_{\phi\phi}$, but also on the global magnetic-field configuration around the BH, either via the magnetic field components $\hat{\mathcal{B}}^{(\alpha)}$, or through the field strength given by $\hat{v}_{\perp} = \mathcal{E}/\mathcal{B}$. In addition, the dynamics of the bulk plasma is encoded in \hat{v}_{\parallel} , that

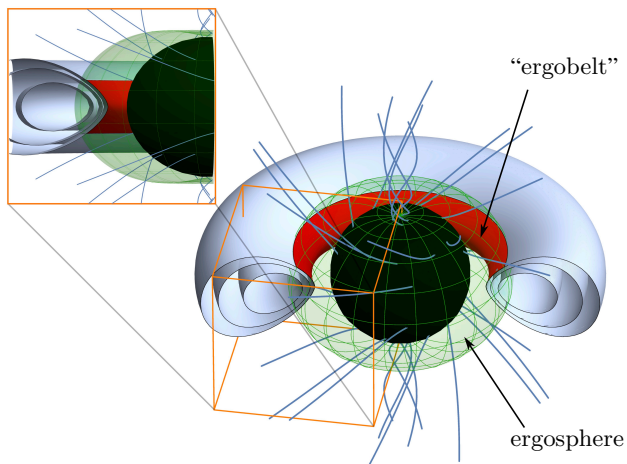


Figure 1. Shown with grey contours are the iso-levels of the rest-mass density of a torus with a toroidal magnetic field entering the BH ergosphere (green region). Reconnection and plasmoid production can take place on the surface of the torus and if this happens in the ergoregion, i.e., on the “ergobelt” (red region), then a PP can be activated from plasmoids having a negative energy-at-infinity.

should be prescribed together with the coordinate invariant quantities $\Psi(r, \theta)$, $I(r, \theta)$, and $\Omega(\Psi)$. Note that Eq. (15) is consistent with any stationary and axisymmetric solution in ideal MHD and in FFE, and can be used to model BH-energy extraction by plasmoids in more realistic configurations. By contrast, previous models were restricted to the equatorial plane and invoked a Keplerian dynamics not realistic within the ergosphere (Koide & Arai 2008; Asenjo & Comisso 2017; Comisso & Asenjo 2021).

3. APPLICATION TO A MAGNETISED TORUS

All studies to date of reconnection-driven PP have been restricted to scenarios where current-sheets develop on the BH equatorial plane. However, there is growing numerical evidence, either from MHD (Mahlmann et al. 2020; Ripperda et al. 2020; Nathanail et al. 2020, 2021; Ripperda et al. 2022; Dimitropoulos et al. 2024) or from PIC simulations (El Mellah et al. 2022, 2023; Vos et al. 2024), that significant reconnection takes place also in the transition zone between the thick accretion disc and the ensuing jet launched by the BH. More specifically, such simulations have shown that the accretion disc around BHs develops a toroidal component and that the transition region between the torus and the funnel systematically leads to reconnection phenomena.

To achieve a treatment in which the off-equatorial dynamics of matter is not prescribed “by hand” (as done so far with equatorial current sheets) but follows self-consistently from a stable fluid configuration, we apply our general treatment to well-known Komissarov’s solution, namely, to a geometrically thick disc endowed with purely toroidal magnetic fields corotating with the BH (Komissarov 2006; Montero et al. 2007; Gimeno-Soler & Font 2017). The pres-

ence of an inner light surface will naturally lead to dominant toroidal magnetospheric fields in the ergoregion with polarity in the counterrotating direction (Komissarov 2004; Uzdensky 2005; Nathanail & Contopoulos 2014; Gralla & Jacobson 2014; Camilloni et al. 2022). Indeed, a necessary condition for the BZ mechanism to occur is $\omega_{\text{BH}} > \Omega > 0$ (Lasota et al. 2014). This implies that the field lines tension oppose to the BH rotation, so that the azimuthal components of the magnetic field must have polarity in the counter-rotating direction, $\hat{\mathcal{B}}^{(Y)} = \sqrt{\gamma_{\phi\phi}}\hat{\mathcal{B}}^{\phi} \propto -I \propto -(\omega_{\text{BH}} - \Omega) < 0$ close to the horizon (see, for instance, Camilloni et al. 2022, for a derivation).

Hence, with the simultaneous presence of toroidal magnetic fields with corotating polarity within the torus and toroidal magnetospheric fields with counterrotating polarity within the funnel, the accretion-disc surface will develop a current-sheet and act as an optimal site for the production plasmoids, as also found in numerical simulations (Dimitropoulos et al. 2024)⁴. Furthermore, the portion of the torus surface that is inside the ergosphere and undergoes reconnection, i.e., what we dub “ergobelt” (red region in Fig. 1), can generate plasmoids that have negative energy-at-infinity and hence tap the BH rotational energy via a plasmoid-driven PP. Note that the current sheet on the torus surface will also be accompanied by the standard equatorial current-sheet that inevitably develops for split-field configurations; we refer to Koide & Arai (2008); Asenjo & Comisso (2017); Comisso & Asenjo (2021); Parfrey et al. (2019); Chen et al. (2024) to review the phenomenology and energetics associated to these current sheets.

Such a magnetised torus, thus, provides a simplified but non-trivial configuration that is mathematically self-consistent and does not invoke unrealistic assumptions. The Komissarov solution naturally entails that $\Psi = 0$ and

$$\hat{v}_{\parallel} = \ell_0 \frac{\alpha}{\sqrt{\gamma_{\phi\phi}(\omega_z \ell_0 - 1)}}, \quad (16)$$

so that $\hat{v}_{\perp} = 0$ and $\hat{\mathcal{B}}^{(X)} = \hat{\mathcal{B}}^{(Z)} = 0$ (see Appendix). Hereafter we will consider maximally-filled tori with $\ell_0 \approx \ell_{\text{mb}}$ and $\mathcal{W}_{\text{in}} = \mathcal{W}_{\text{cusp}} = 0$.

Following Koide & Arai (2008) and Comisso & Asenjo (2021), we assume the plasmoids/RAIBs to consist of relativistically-hot plasma described by an ideal-fluid equation of state so that $H = 4U(\Gamma - 1)$. As mentioned above, and since we are interested in the PP associated with an accretion scenario onto a supermassive black hole, the reconnection we envisage to take place at the ergobelt is one that

⁴ Under realistic conditions of accretion and outside the ergosphere, the magnetic field will also have a poloidal component both in the torus and in the jet, so that the presence of guide fields can be relevant for reconnection taking place far from the ergosphere.

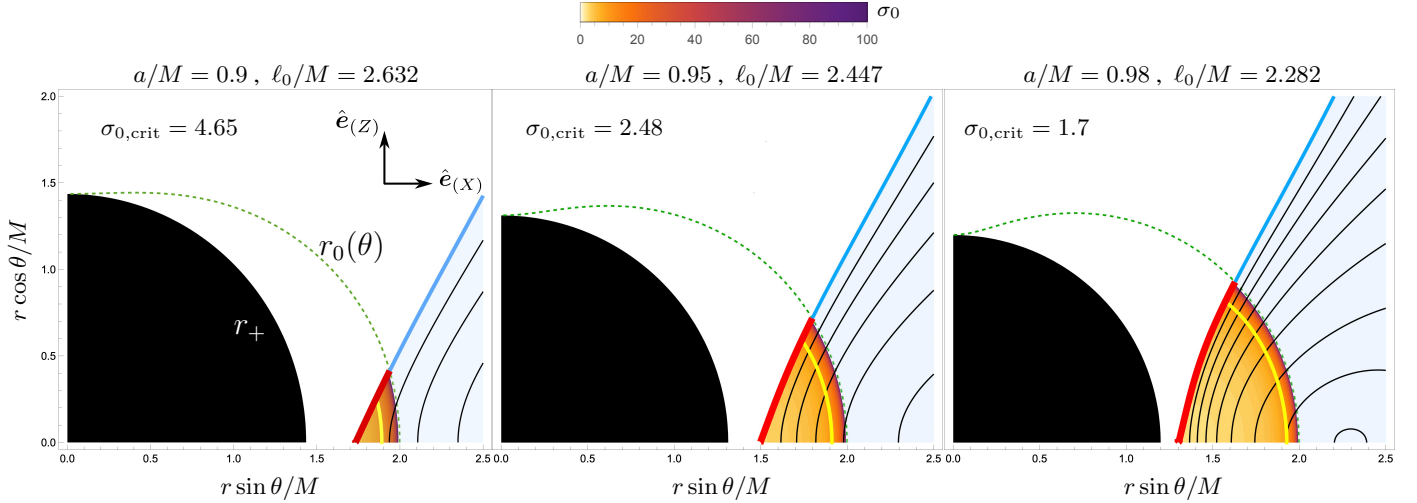


Figure 2. Polar sections of tori with $\ell_0 \simeq \ell_{\text{mb}}$ (light blue shading) entering the ergosphere r_0 (green dashed line), with BH spin increasing from left to right. The torus surface inside the ergosphere, dubbed ergobelt (red solid line), is suitable for reconnection to drive a PP. The colormap reports values of the magnetisation σ_0 necessary for the pair-production of plasmoids with $\varepsilon_+^\infty > 0$ and $\varepsilon_-^\infty < 0$ at different positions in the torus, with the yellow solid line marking $\sigma_0 = 10$.

involves a hydrogen plasma. Moreover, we use the analytic model of magnetic reconnection by Liu et al. (2017), with a reconnection electric field proportional to the reconnection rate, and predicting plasmoid velocities that are simple functions of the magnetisation $\sigma_0 := b^2/w_0$, where w_0 is the enthalpy density. More specifically, we set (Lyubarsky 2005)

$$\tilde{v}_{\text{out}} \approx \sqrt{\sigma_0/(1+\sigma_0)}, \quad \tilde{\gamma}_{\text{out}} \approx \sqrt{1+\sigma_0}, \quad (17)$$

so that Eq. (15) simplifies and becomes dependent on the BH spin a , the plasma magnetisation⁵ σ_0 , the torus angular momentum ℓ_0 , and the (r, θ) location of the ergobelt (see Eq. (C8) in the Appendix).

A number of important remarks should be made on ε_\pm^∞ as obtained above. First, the value at the horizon, $\varepsilon_\pm^\infty|_{r_+}$, is finite for all BH spins. Second, since the conditions for a successful PP require $\varepsilon_+^\infty > 0$ and $\varepsilon_-^\infty < 0$ (Comisso & Asenjo 2021), a critical magnetisation $\sigma_{0,\text{crit}}$ exists that depends on the BH spin and torus properties and below which no PP can take place. For instance, for $a/M = 0.9$ and $\ell_0/M \lesssim 2.63$, $\sigma_{0,\text{crit}} \approx 4.65$, which is consistent with the values observed in the transition region in simulations (Nathanail et al. 2020, 2021). Third, in regions where $\sigma_0 \gg 1$, Eq. (15) further simplifies to

$$\varepsilon_\pm^\infty = \sqrt{\sigma_0} \left(1 \pm \frac{\sqrt{\gamma\phi\phi}}{\alpha} \omega_z \right) \sqrt{\frac{1 \pm \hat{v}_\parallel}{1 \mp \hat{v}_\parallel}}, \quad (18)$$

⁵ Typical magnetisation just inside the torus is $\sim \mathcal{O}(0.01 - 0.1)$ with vanishing magnetic fields at the surface. Numerical simulations show that σ_0 jumps to $\sim \mathcal{O}(10 - 100)$ just outside the torus (Mahlmann et al. 2020; Ripperda et al. 2020; Nathanail et al. 2020, 2021; Ripperda et al. 2022; Dimitropoulos et al. 2024). Hence, to model the reconnection in the transition region in the vicinity of the ergobelt we consider $0.1 \lesssim \sigma_0 \lesssim 10$.

showing that plasmoids with $\varepsilon_-^\infty < 0$ can be produced for sufficiently high magnetisation, provided that a portion of the torus intersects the ergosphere where $\omega_z \sqrt{\gamma\phi\phi} \geq \alpha$. For maximally filled tori, the torus cusp is inside the ergosphere if

$$a > a_{\text{crit}} := 2(\sqrt{2} - 1)M \approx 0.83M. \quad (19)$$

Finally, and most importantly, because Eq. (15) applied to a torus is not restricted to the equatorial plane, it allows us to study for the first time the problem plasmoid-driven PP in an axisymmetric but non-equatorial context.

Figure 2 shows polar sections of magnetised tori with $\ell_0 \lesssim \ell_{\text{mb}}$ entering the ergosphere of BHs with spin. Marked with a colormap are the values of the magnetisation σ_0 such that $\varepsilon_+^\infty > 0$ and $\varepsilon_-^\infty < 0$ [cf. Eq. (15)] and reported are corresponding the critical value for the magnetisation increasing from left to right. For magnetisations above a critical value $\sigma_{0,\text{crit}}$, the innermost part of the torus possesses an ergobelt as a site for the production of plasmoids with negative energy-at-infinity and hence yield a PP. Moreover, for faster spinning BHs, larger portions of the torus penetrate the ergosphere increasing the potential production of plasmoids.

3.1. Energetics of the plasmoid-driven PP

Because of the nonlinear nature of reconnection and of the plasma dynamics near the torus surface, the energy extraction process will be intrinsically stochastic, so that the energy-extraction rate \dot{E}_{rec} will depend on the local reconnection rate, routinely assumed to be $\mathcal{R}_{\text{rec}} \simeq 0.1$ (Liu et al. 2017; Cassak et al. 2017; Huang & Bhattacharjee 2012; Asenjo & Comisso 2017; Comisso & Asenjo 2021). Taking now \mathcal{L} and \mathcal{A} respectively as the linear size and surface area of the ergobelt (note there are two ergobelts, symmetric with respect

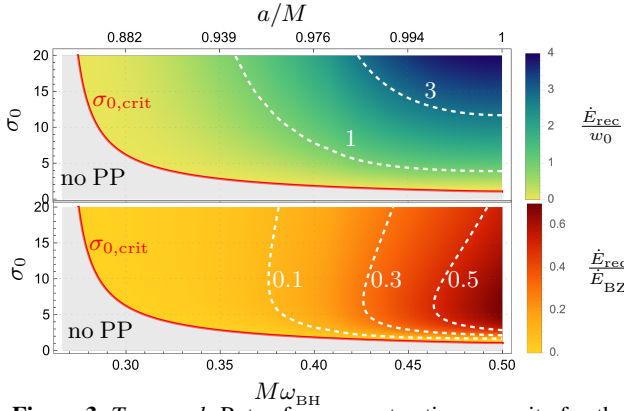


Figure 3. *Top panel:* Rate of energy extraction per unit of enthalpy density, \dot{E}_{rec}/w_0 , at the ergobelt of a maximally-filling torus as a function of the magnetisation σ_0 and BH angular velocity ω_{BH} (the top horizontal axis uses instead a scale in a/M). The red solid line marks the critical magnetisation $\sigma_{0,\text{crit}}$ below which no PP is possible (grey shaded area). *Bottom panel:* The same as in the top but when the energy extraction rate is normalised to the BZ power $\dot{E}_{\text{rec}}/\dot{E}_{\text{BZ}}$.

to the equatorial plane), we approximate the enthalpy density as $w_0 \approx H/(\mathcal{L}\mathcal{A})$ and express the energy extraction rate as

$$\dot{E}_{\text{rec}} = -2 \mathcal{R}_{\text{rec}} w_0 \int_{\mathcal{A}} \varepsilon_{-}^{\infty} d\mathcal{A} = -2 \mathcal{R}_{\text{rec}} w_0 \mathcal{A} \langle \varepsilon_{-}^{\infty} \rangle, \quad (20)$$

where

$$\langle \varepsilon_{-}^{\infty} \rangle := \frac{\int_{\mathcal{A}} \varepsilon_{-}^{\infty} d\mathcal{A}}{\int_{\mathcal{A}} d\mathcal{A}}, \quad (21)$$

is the energy-at-infinity averaged over the area of the ergobelt (see Appendix).

In the top part of Fig. 3 we report the behaviour of \dot{E}_{rec}/w_0 as a function of the plasma magnetisation and BH spin. As expected, no energy extraction occurs if the BH is not spinning sufficiently fast (the torus does not enter the ergosphere) or if the magnetisation is below the corresponding critical value (red solid line). Conversely, the process is more efficient for rapidly spinning BHs and high magnetisations, since the effective area of the ergobelt then increases. The values of \dot{E}_{rec} are comparable or larger than those estimated by Comisso & Asenjo (2021) for plasmoids generated in the equatorial plane.

Finally, we can compare the extracted energy via plasmoids with the power extracted via the BZ mechanism, which, we recall, is steady and effective for any nonzero value of the BH spin. The BZ power extracted by a split-monopole field in Kerr can be written as an expansion in the BH angular velocity, $\omega_{\text{BH}} := \omega_z|_{r_+}$, to ensure a better convergence (Tchekhovskoy et al. 2010; Camilloni et al. 2022), and reads

$$\dot{E}_{\text{BZ}} \simeq \left(\frac{2\pi B_0^2 r_+^2 \omega_{\text{BH}}^2}{3} \right) [1 + 1.38 (M\omega_{\text{BH}})^2 - 9.2 (M\omega_{\text{BH}})^4], \quad (22)$$

where, for simplicity, we assumed that the magnetic field at the event horizon is comparable to that at the ergobelt, i.e., $B_{r=r_+}^2 \approx B_0^2 = \sigma_0 w_0$, and where the magnetic flux across the horizon is given by $\Phi_{\text{H}} \approx 4\pi B_0 r_+^2$. The bottom part of Fig. 3 reports the ratio $\dot{E}_{\text{rec}}/\dot{E}_{\text{BZ}}$ showing that for sufficiently large BH spins and magnetisations, the plasmoid-driven PP leads to an energy extraction that is smaller but comparable to that associated with the BZ mechanism. Figure 3 invites a comparison with Fig. (7) in Comisso & Asenjo (2021), where $\dot{E}_{\text{rec}}/\dot{E}_{\text{BZ}}$ was also computed assuming plasmoids generated from an equatorial current sheet and having Keplerian velocities. When making such a comparison, we should take into account differences in the physical regimes considered and in the approximations made. In particular, since we consider an accretion scenario, we limit the magnetisation to regimes that are compatible with the simulations and hence consider $\sigma_0 \lesssim 20$ [Comisso & Asenjo (2021) consider instead $\sigma_0 \lesssim 10^6$]. Furthermore, the magnetic flux considered by Comisso & Asenjo (2021) includes a factor proportional to $\sin \xi$, where ξ is the ‘‘orientation angle’’, that is, the angle between the radial and azimuthal directions of the plasmoid velocity as measured in the comoving frame. The inclusion of this angular dependence, which is unusual for a surface-integrated flux that should not depend on the orientation angle, decreases the BZ power by a factor $\sin^2 \xi$, thus magnifying the ratio by ~ 15 for $\xi = \pi/12$ [which is the value considered in Fig. (7) of Comisso & Asenjo (2021)]. When ignoring this factor and considering similar values of magnetisation, our estimates of $\dot{E}_{\text{rec}}/\dot{E}_{\text{BZ}}$ are comparable to those computed by Comisso & Asenjo (2021) and by Parfrey et al. (2019) for electrons undergoing a PP.

4. CONCLUSIONS

Responding to the increasing evidence that resistive effects in plasmas around BHs play an important role in shaping the observed phenomenology of these objects, we have presented a general approach to the study of a PP driven by plasmoids produced at reconnection sites along current sheets. Our formalism ultimately establishes the physical conditions to make a plasmoid-driven PP energetically viable and can be applied equally to scenarios that are dominated by the plasma or by the magnetic field, that is, in MHD or FFE regimes. It is also genuinely multidimensional and hence allows one to explore conditions that are beyond the ones studied so far and that have been restricted to the equatorial plane. In this sense, it provides a direct contact with numerical simulations, either in MHD (Mahlmann et al. 2020; Ripperda et al. 2020; Nathanail et al. 2020, 2021; Ripperda et al. 2022; Dimitropoulos et al. 2024) or with PIC approaches (Parfrey et al. 2019; El Mellah et al. 2022, 2023; Vos et al. 2024), all of which highlight an intense reconnection activity outside the equatorial plane. Finally, it does not assume an ad-hoc

description of the dynamics of the plasma, or conjecture its kinematic properties with oversimplified and possibly unrealistic configurations. On the contrary, it constructs the dynamics of the plasma starting from a well-known configuration, that of an equilibrium torus with a toroidal magnetic field, and thus possessing all the features necessary to compute self-consistently the reconnection process and estimate the PP energetics.

While the results presented here offer the first coherent approach to a multidimensional treatment of the PP driven by magnetic reconnection, they can be improved in a number of ways. First, by developing a more accurate descriptions of plasmoids that could overcome the limitations of the RAIB model. Second, by exploiting the results of numerical simulations to produce better estimates of the reconnection rate and hence of the efficiency of the energy-extraction process. Thirdly, by connecting the plasmoid production at the ergobelt with the plasmoid production on the equatorial plane (that

remains a favourable site for the production of plasmoids), hence join the MHD regime of the plasma in the torus with the FFE regime when the plasma has left the torus and is accreting onto the BH. We plan to investigate these important aspects in future works.

ACKNOWLEDGEMENTS

We thank Benoît Cerutti, Luca Comisso, Ileyk El Mellah, Claudio Meringolo, Antonios Nathanail, and Kyle Parfrey for insightful discussions and comments. Partial funding comes from the State of Hesse within the Research Cluster ELEMENTS (Project ID 500/10.006), by the ERC Advanced Grant “JETSET: Launching, propagation and emission of relativistic jets from binary mergers and across mass scales” (Grant No. 884631). LR acknowledges the Walter Greiner Gesellschaft zur Förderung der physikalischen Grundlagenforschung e.V. through the Carl W. Fueck Laureatus Chair.

REFERENCES

- Abramowicz, M., Jaroszynski, M., & Sikora, M. 1978, *Astron. Astrophys.*, 63, 221
- Aimar, N., Dmytriiev, A., Vincent, F. H., et al. 2023, *Astron. Astrophys.*, 672, A62, doi: [10.1051/0004-6361/202244936](https://doi.org/10.1051/0004-6361/202244936)
- Akiyama, K., & et al. 2019, *Astrophys. J. Lett.*, 875, L5, doi: [10.3847/2041-8213/ab0f43](https://doi.org/10.3847/2041-8213/ab0f43)
- Anderson, M., Hirschmann, E. W., Lehner, L., et al. 2008, *Phys. Rev. Lett.*, 100, 191101, doi: [10.1103/PhysRevLett.100.191101](https://doi.org/10.1103/PhysRevLett.100.191101)
- Asenjo, F. A., & Comisso, L. 2015, *Phys. Rev. Lett.*, 114, 115003, doi: [10.1103/PhysRevLett.114.115003](https://doi.org/10.1103/PhysRevLett.114.115003)
- . 2017, *Phys. Rev. Lett.*, 118, 055101, doi: [10.1103/PhysRevLett.118.055101](https://doi.org/10.1103/PhysRevLett.118.055101)
- Bañados, M., Silk, J., & West, S. M. 2009, *Phys. Rev. Lett.*, 103, 111102, doi: [10.1103/PhysRevLett.103.111102](https://doi.org/10.1103/PhysRevLett.103.111102)
- Ball, D., Özel, F., Psaltis, D., Chan, C.-K., & Sironi, L. 2018, *Astrophys. J.*, 853, 184, doi: [10.3847/1538-4357/aaa42f](https://doi.org/10.3847/1538-4357/aaa42f)
- Bardeen, J. M., Press, W. H., & Teukolsky, S. A. 1972, *Astrophys. J.*, 178, 347, doi: [10.1086/151796](https://doi.org/10.1086/151796)
- Bejger, M., Piran, T., Abramowicz, M., & Håkanson, F. 2012, *Phys. Rev. Lett.*, 109, 121101, doi: [10.1103/PhysRevLett.109.121101](https://doi.org/10.1103/PhysRevLett.109.121101)
- Beloborodov, A. M. 2017, *The Astrophysical Journal*, 850, 141, doi: [10.3847/1538-4357/aa8f4f](https://doi.org/10.3847/1538-4357/aa8f4f)
- Berti, E., Brito, R., & Cardoso, V. 2015, *Phys. Rev. Lett.*, 114, 251103, doi: [10.1103/PhysRevLett.114.251103](https://doi.org/10.1103/PhysRevLett.114.251103)
- Blandford, R. D., & Znajek, R. L. 1977, *Mon. Not. Roy. Astron. Soc.*, 179, 433, doi: [10.1093/mnras/179.3.433](https://doi.org/10.1093/mnras/179.3.433)
- Bosch, P., Green, S. R., & Lehner, L. 2016, *Phys. Rev. Lett.*, 116, 141102, doi: [10.1103/PhysRevLett.116.141102](https://doi.org/10.1103/PhysRevLett.116.141102)
- Bransgrove, A., Ripperda, B., & Philippov, A. 2021, *Phys. Rev. Lett.*, 127, 055101, doi: [10.1103/PhysRevLett.127.055101](https://doi.org/10.1103/PhysRevLett.127.055101)
- Camilloni, F., Dias, O. J. C., Grignani, G., et al. 2022, *JCAP*, 07, 032, doi: [10.1088/1475-7516/2022/07/032](https://doi.org/10.1088/1475-7516/2022/07/032)
- Cassak, P. A., Liu, Y. H., & Shay, M. A. 2017, *J. Plasma Phys.*, 83, 715830501, doi: [10.1017/S0022377817000666](https://doi.org/10.1017/S0022377817000666)
- Chael, A., Lupsasca, A., Wong, G. N., & Quataert, E. 2023, *Astrophys. J.*, 958, 65, doi: [10.3847/1538-4357/acf92d](https://doi.org/10.3847/1538-4357/acf92d)
- Chen, B., Hou, Y., Li, J., & Shen, Y. 2024, *Phys. Rev. D*, 110, 063003, doi: [10.1103/PhysRevD.110.063003](https://doi.org/10.1103/PhysRevD.110.063003)
- Comisso, L., & Asenjo, F. A. 2014, *Phys. Rev. Lett.*, 113, 045001, doi: [10.1103/PhysRevLett.113.045001](https://doi.org/10.1103/PhysRevLett.113.045001)
- . 2021, *Phys. Rev. D*, 103, 023014, doi: [10.1103/PhysRevD.103.023014](https://doi.org/10.1103/PhysRevD.103.023014)
- Crinquand, B., Cerutti, B., Dubus, G., Parfrey, K., & Philippov, A. 2022, *Phys. Rev. Lett.*, 129, 205101, doi: [10.1103/PhysRevLett.129.205101](https://doi.org/10.1103/PhysRevLett.129.205101)
- Dadhich, N., Tursunov, A., Ahmedov, B., & Stuchlík, Z. 2018, *Mon. Not. R. Astron. Soc.*, 478, L89, doi: [10.1093/mnras/sly073](https://doi.org/10.1093/mnras/sly073)
- Dimitropoulos, I., Nathanail, A., Petropoulou, M., & Contopoulos, I. 2024, preprint, doi: [10.48550/arXiv.2407.14312](https://doi.org/10.48550/arXiv.2407.14312)
- Dionysopoulou, K., Alic, D., & Rezzolla, L. 2015, *Phys. Rev. D*, 92, 084064, doi: [10.1103/PhysRevD.92.084064](https://doi.org/10.1103/PhysRevD.92.084064)
- East, W. E., & Pretorius, F. 2017, *Phys. Rev. Lett.*, 119, 041101, doi: [10.1103/PhysRevLett.119.041101](https://doi.org/10.1103/PhysRevLett.119.041101)
- El Mellah, I., Cerutti, B., & Crinquand, B. 2023, *Astron. Astrophys.*, 677, A67, doi: [10.1051/0004-6361/202346781](https://doi.org/10.1051/0004-6361/202346781)

- El Mellah, I., Cerutti, B., Crinquand, B., & Parfrey, K. 2022, *Astron. Astrophys.*, 663, A169, doi: [10.1051/0004-6361/202142847](https://doi.org/10.1051/0004-6361/202142847)
- Event Horizon Telescope Collaboration, Akiyama, K., et al. 2022, *Astrophys. J. Lett.*, 930, L16, doi: [10.3847/2041-8213/ac6672](https://doi.org/10.3847/2041-8213/ac6672)
- Fan, Z.-Y., Li, Y., Zhou, F., & Guo, M. 2024, *Phys. Rev. D*, 110, 104044, doi: [10.1103/PhysRevD.110.104044](https://doi.org/10.1103/PhysRevD.110.104044)
- Gelles, Z., Chael, A., & Quataert, E. 2024, preprint, doi: [10.48550/arXiv.2410.009542](https://doi.org/10.48550/arXiv.2410.009542)
- Gimeno-Soler, S., & Font, J. A. 2017, *Astron. Astrophys.*, 607, A68, doi: [10.1051/0004-6361/201730935](https://doi.org/10.1051/0004-6361/201730935)
- Gralla, S. E., & Jacobson, T. 2014, *Mon. Not. Roy. Astron. Soc.*, 445, 2500, doi: [10.1093/mnras/stu1690](https://doi.org/10.1093/mnras/stu1690)
- Guo, F., Li, H., Daughton, W., & Liu, Y.-H. 2014, *Phys. Rev. Lett.*, 113, 155005, doi: [10.1103/PhysRevLett.113.155005](https://doi.org/10.1103/PhysRevLett.113.155005)
- Huang, Y.-M., & Bhattacharjee, A. 2012, *Phys. Rev. Lett.*, 109, 265002, doi: [10.1103/PhysRevLett.109.265002](https://doi.org/10.1103/PhysRevLett.109.265002)
- Kiuchi, K., Sekiguchi, Y., Kyutoku, K., et al. 2015, *Phys. Rev. D*, 92, 064034, doi: [10.1103/PhysRevD.92.064034](https://doi.org/10.1103/PhysRevD.92.064034)
- Koide, S., & Arai, K. 2008, *Astrophys. J.*, 682, 1124, doi: [10.1086/589497](https://doi.org/10.1086/589497)
- Komissarov, S. S. 2004, *Mon. Not. R. Astron. Soc.*, 350, 427, doi: [10.1111/j.1365-2966.2004.07598.x](https://doi.org/10.1111/j.1365-2966.2004.07598.x)
- . 2006, *Mon. Not. R. Astron. Soc.*, 368, 993, doi: [10.1111/j.1365-2966.2006.10183.x](https://doi.org/10.1111/j.1365-2966.2006.10183.x)
- Kozłowski, M., Jaroszynski, M., & Abramowicz, M. A. 1978, *Astron. and Astrophys.*, 63, 209
- Landau, L. D., & Lifshitz, E. M. 2004, *The Classical Theory of Fields*, Course of Theoretical Physics, Volume 2 (Oxford: Elsevier Butterworth-Heinemann)
- Lasota, J. P., Gourgoulhon, E., Abramowicz, M., Tchekhovskoy, A., & Narayan, R. 2014, *Phys. Rev. D*, 89, 024041, doi: [10.1103/PhysRevD.89.024041](https://doi.org/10.1103/PhysRevD.89.024041)
- Liu, Y.-H., Guo, F., Daughton, W., Li, H., & Hesse, M. 2015, *Phys. Rev. Lett.*, 114, 095002, doi: [10.1103/PhysRevLett.114.095002](https://doi.org/10.1103/PhysRevLett.114.095002)
- Liu, Y.-H., Hesse, M., Guo, F., et al. 2017, *Phys. Rev. Lett.*, 118, 085101, doi: [10.1103/PhysRevLett.118.085101](https://doi.org/10.1103/PhysRevLett.118.085101)
- Liu, Y. T., Shapiro, S. L., Etienne, Z. B., & Taniguchi, K. 2008, *Phys. Rev. D*, 78, 024012, doi: [10.1103/PhysRevD.78.024012](https://doi.org/10.1103/PhysRevD.78.024012)
- Lyubarsky, Y. E. 2005, *Mon. Not. Roy. Astr. Soc.*, 358, 113, doi: [10.1111/j.1365-2966.2005.08767.x](https://doi.org/10.1111/j.1365-2966.2005.08767.x)
- Mahlmann, J. F., Levinson, A., & Aloy, M. A. 2020, *Mon. Not. R. Astron. Soc.*, 494, 4203, doi: [10.1093/mnras/staa943](https://doi.org/10.1093/mnras/staa943)
- McKinney, J. C. 2006, *Mon. Not. Roy. Astron. Soc.*, 367, 1797, doi: [10.1111/j.1365-2966.2006.10087.x](https://doi.org/10.1111/j.1365-2966.2006.10087.x)
- Meringolo, C., Cruz-Osorio, A., Rezzolla, L., & Servidio, S. 2023, *Astrophys. J.*, 944, 122, doi: [10.3847/1538-4357/acaefe](https://doi.org/10.3847/1538-4357/acaefe)
- Mizuno, Y., & Rezzolla, L. 2024, arXiv e-prints, arXiv:2404.13824, doi: [10.48550/arXiv.2404.13824](https://doi.org/10.48550/arXiv.2404.13824)
- Montero, P. J., Zanotti, O., Font, J. A., & Rezzolla, L. 2007, *Mon. Not. R. Astron. Soc.*, 378, 1101, doi: [10.1111/j.1365-2966.2007.11844.x](https://doi.org/10.1111/j.1365-2966.2007.11844.x)
- Nathanail, A., & Contopoulos, I. 2014, *Astrophys. J.*, 788, 186, doi: [10.1088/0004-637X/788/2/186](https://doi.org/10.1088/0004-637X/788/2/186)
- Nathanail, A., Fromm, C. M., Porth, O., et al. 2020, *Mon. Not. R. Astron. Soc.*, 495, 1549, doi: [10.1093/mnras/staa1165](https://doi.org/10.1093/mnras/staa1165)
- Nathanail, A., Gill, R., Porth, O., Fromm, C. M., & Rezzolla, L. 2021, *Mon. Not. R. Astron. Soc.*, 502, 1843, doi: [10.1093/mnras/stab115](https://doi.org/10.1093/mnras/stab115)
- Palenzuela, C., Lehner, L., Ponce, M., et al. 2013, *Phys. Rev. Lett.*, 111, 061105, doi: [10.1103/PhysRevLett.111.061105](https://doi.org/10.1103/PhysRevLett.111.061105)
- Palenzuela, C., Lehner, L., Reula, O., & Rezzolla, L. 2009, *Mon. Not. R. Astron. Soc.*, 394, 1727, doi: [10.1111/j.1365-2966.2009.14454.x](https://doi.org/10.1111/j.1365-2966.2009.14454.x)
- Pani, P., Cardoso, V., Gualtieri, L., Berti, E., & Ishibashi, A. 2012, *Phys. Rev. Lett.*, 109, 131102, doi: [10.1103/PhysRevLett.109.131102](https://doi.org/10.1103/PhysRevLett.109.131102)
- Parfrey, K., Philippov, A., & Cerutti, B. 2019, *Phys. Rev. Lett.*, 122, 035101, doi: [10.1103/PhysRevLett.122.035101](https://doi.org/10.1103/PhysRevLett.122.035101)
- Penrose, R., & Floyd, R. M. 1971, *Nature*, 229, 177, doi: [10.1038/physci229177a0](https://doi.org/10.1038/physci229177a0)
- Press, W. H., & Teukolsky, S. A. 1972, *Nature*, 238, 211, doi: [10.1038/238211a0](https://doi.org/10.1038/238211a0)
- Rezzolla, L., Giacomazzo, B., Baiotti, L., et al. 2011, *Astrophys. J. Letters*, 732, L6, doi: [10.1088/2041-8205/732/1/L6](https://doi.org/10.1088/2041-8205/732/1/L6)
- Rezzolla, L., & Zanotti, O. 2013, *Relativistic Hydrodynamics* (Oxford University Press), doi: [10.1093/acprof:oso/9780198528906.001.0001](https://doi.org/10.1093/acprof:oso/9780198528906.001.0001)
- Ripperda, B., Bacchini, F., & Philippov, A. A. 2020, *Astrophys. J.*, 900, 100, doi: [10.3847/1538-4357/ababab](https://doi.org/10.3847/1538-4357/ababab)
- Ripperda, B., Liska, M., Chatterjee, K., et al. 2022, *Astrophys. J. Lett.*, 924, L32, doi: [10.3847/2041-8213/ac46a1](https://doi.org/10.3847/2041-8213/ac46a1)
- Ripperda, B., Bacchini, F., Porth, O., et al. 2019, *Astrophys. J., Supp.*, 244, 10, doi: [10.3847/1538-4365/ab3922](https://doi.org/10.3847/1538-4365/ab3922)
- Ruffini, R., Prakapenia, M., Quevedo, H., & Zhang, S. 2024, Accepted in *Phys. Rev. Lett.* <https://arxiv.org/abs/2405.08229>
- Schnittman, J. D. 2014, *Phys. Rev. Lett.*, 113, 261102, doi: [10.1103/PhysRevLett.113.261102](https://doi.org/10.1103/PhysRevLett.113.261102)
- Shen, Y., & YuChih, H.-Y. 2024, arXiv e-prints, arXiv:2412.03010, doi: [10.48550/arXiv.2412.03010](https://doi.org/10.48550/arXiv.2412.03010)
- Su, Y., Veronig, A. M., Holman, G. D., et al. 2013, *Nature Physics*, 9, 489
- Tchekhovskoy, A., Narayan, R., & McKinney, J. C. 2010, *Astrophys. J.*, 711, 50, doi: [10.1088/0004-637X/711/1/50](https://doi.org/10.1088/0004-637X/711/1/50)
- Thorne, K. S., & Macdonald, D. 1982, *Mon. Not. R. Astr. Soc.*, 198, 339
- Uzdensky, D. A. 2005, *Astrophys. J.*, 620, 889, doi: [10.1086/427180](https://doi.org/10.1086/427180)

Uzdensky, D. A., & Spitkovsky, A. 2013, *The Astrophysical Journal*, 780, 3, doi: [10.1088/0004-637X/780/1/3](https://doi.org/10.1088/0004-637X/780/1/3)

Vos, J., Cerutti, B., Moscibrodzka, M., & Parfrey, K. 2024, preprint, doi: [10.48550/arXiv.2410.19061](https://doi.org/10.48550/arXiv.2410.19061)

Yamada, M., Kulsrud, R., & Ji, H. 2010, *Rev. Mod. Phys.*, 82, 603, doi: [10.1103/RevModPhys.82.603](https://doi.org/10.1103/RevModPhys.82.603)

Zweibel, E. G., & Yamada, M. 2009, *Annual Review of Astronomy and Astrophysics*, 47, 291, doi: <https://doi.org/10.1146/annurev-astro-082708-101726>

APPENDIX

In what follows we provide the most important details about the calculations or considerations that are needed to obtain the results presented in the main text.

A. KERR METRIC AND ZAMO FRAME.

The Kerr metric in Boyer-Lindquist (BL) coordinates $x^\mu = (t, r, \theta, \phi)$ and in a $(3+1)$ -form reads $ds^2 = g_{\mu\nu} dx^\mu dx^\nu = -\alpha^2 dt^2 + \gamma_{ij}(dx^i + \beta^i dt)(dx^j + \beta^j dt)$ with the lapse function, the shift vector and the absolute space metric respectively defined as

$$\alpha = \frac{1}{\sqrt{-g^{tt}}} = \sqrt{\frac{\Delta\Sigma}{\Pi}}, \quad \beta^i = \alpha^2 g^{ti} = -\alpha^2 \frac{2Mar}{\Delta\Sigma} \delta_\phi^i, \quad \gamma_{ij} dx^i dx^j = \Sigma/\Delta dr^2 + \Sigma d\theta^2 + \Pi/\Sigma \sin^2 \theta d\phi^2, \quad (\text{A1})$$

and the metric determinant decomposes as $g = -\alpha^2 \det(\gamma_{ij})$. The metric functions explicitly read $\Delta = r^2 - 2Mr + a^2$, $\Sigma = r^2 + a^2 \cos^2 \theta$ and $\Pi = (r^2 + a^2)^2 - a^2 \Delta \sin^2 \theta$, with the event horizon position given by the r_+ root of $\Delta = (r-r_+)(r-r_-)$, $r_\pm = M(1 \pm \sqrt{1 - a_*^2})$, and the ergosphere location at $r_0(\theta) = M(1 + \sqrt{1 - a_*^2 \cos^2 \theta})$, where $a_* := a/M$. We assume the BH to have $0 \leq a_* \leq 1$, with the upper bound imposed by the cosmic censorship conjecture. Other interesting locations in the BH equatorial plane, $\theta = \pi/2$, are given by the marginally stable corotating (+) and counter-rotating (-) circular orbit, $r_{\text{ms},\pm}$, and by the marginally bound circular orbit $r_{\text{ms},\pm}$, depicted in Fig. 4.

The ZAMO is a normal observer (the corresponding 1-form in BL coordinates is $\boldsymbol{\eta} = -\alpha d\mathbf{t}$), with an associated local Cartesian right-handed frame $\hat{\mathbf{e}}_{(\alpha)} = (\hat{\mathbf{e}}_{(T)}, \hat{\mathbf{e}}_{(X)}, \hat{\mathbf{e}}_{(Y)}, \hat{\mathbf{e}}_{(Z)})$ specified by the vectors $\hat{\mathbf{e}}_{(T)} = \boldsymbol{\eta}$, $\hat{\mathbf{e}}_{(X)} = \partial_{\mathbf{r}}/\sqrt{\gamma_{rr}}$, $\hat{\mathbf{e}}_{(Y)} = \partial_{\phi}/\sqrt{\gamma_{\phi\phi}}$, and $\hat{\mathbf{e}}_{(Z)} = -\partial_{\theta}/\sqrt{\gamma_{\theta\theta}}$, and form a tetrad, namely, $g_{\mu\nu} = \hat{e}_\mu^{(\alpha)} \hat{e}_\nu^{(\beta)} \hat{\eta}_{(\alpha)(\beta)}$ and $\varepsilon_{\mu\nu\rho\sigma} = \hat{e}_\mu^{(T)} \wedge \hat{e}_\nu^{(X)} \wedge \hat{e}_\rho^{(Y)} \wedge \hat{e}_\sigma^{(Z)}$, where $\hat{\eta}_{(\alpha)(\beta)}$ is the Minkowski metric in the local frame and $\varepsilon_{\mu\nu\rho\sigma} := \sqrt{-g} \eta_{\mu\nu\rho\sigma}$ is the 4-dimensional Levi-Civita tensor.

B. PLASMA VELOCITY.

As mentioned in the main text, the character of the field is set by the invariant quantity $F^{\mu\nu} F_{\mu\nu} = 2(\mathcal{B}^2 - \mathcal{E}^2)$, with the strength of the ZAMO fields given by

$$\mathcal{B}^2 = \frac{1}{\sin^2 \theta} \left[\frac{\Delta(\partial_r \Psi)^2 + (\partial_\theta \Psi)^2}{\Pi} + \frac{I^2}{\Delta} \right], \quad \mathcal{E}^2 = \mathcal{F}^2(\Omega) \frac{\Delta(\partial_r \Psi)^2 + (\partial_\theta \Psi)^2}{\Pi \sin^2 \theta}, \quad (\text{B2})$$

and where we introduced $\mathcal{F}(\Omega) := \sqrt{\gamma_{\phi\phi}}(\omega_z - \Omega)/\alpha$. Notice that $\mathcal{F}(\Omega) = \pm 1$ at the outer/inner light surfaces, i.e., the locations where corotating observers with the field lines become null, $|\partial_t + \Omega(\Psi)\partial_\phi|^2 = \alpha^2(\mathcal{F}^2(\Omega) - 1) = 0$, or equivalently, where the magnetic field transitions from being dominated by poloidal to toroidal components.

The orthonormal vectors (see Eq. (6) in the main text), valid for degenerate fields, are conveniently parameterised in terms of two magnetic orientation angles $\xi_1 := \tan^{-1}(\hat{\mathcal{B}}^{(Y)}/\hat{\mathcal{B}}^{(X)})$ and $\xi_2 := \cos^{-1}(\hat{\mathcal{B}}^{(Z)}/\sqrt{\mathcal{B}^2})$ with respect to the ZAMO frame, such that

$$\begin{aligned} \sin \xi_1 &= -\sqrt{\Pi I}/\sqrt{\Delta(\partial_\theta \Psi)^2 + \Pi I^2}, \\ \sin \xi_2 &= \sqrt{(\Pi I^2 + \Delta(\partial_\theta \Psi)^2)/(\Pi I^2 + \Delta(\Delta(\partial_r \Psi)^2 + (\partial_\theta \Psi)^2))}, \end{aligned} \quad (\text{B3})$$

with explicit expressions given by

$$\begin{aligned} \boldsymbol{\mathcal{X}} &= \mathcal{X}^{(\alpha)} \hat{\mathbf{e}}_{(\alpha)} = (\cos \xi_2/\chi) \hat{\mathbf{e}}_{(X)} - (\cos \xi_1 \sin \xi_2/\chi) \hat{\mathbf{e}}_{(Z)} \\ \boldsymbol{\mathcal{Y}} &= \mathcal{Y}^{(\alpha)} \hat{\mathbf{e}}_{(\alpha)} = \cos \xi_1 \sin \xi_2 \hat{\mathbf{e}}_{(X)} + \sin \xi_1 \sin \xi_2 \hat{\mathbf{e}}_{(Y)} + \cos \xi_2 \hat{\mathbf{e}}_{(Z)}, \\ \boldsymbol{\mathcal{Z}} &= \mathcal{Z}^{(\alpha)} \hat{\mathbf{e}}_{(\alpha)} = -(\cos \xi_1 \sin \xi_1 \sin^2 \xi_2/\chi) \hat{\mathbf{e}}_{(X)} + \chi \hat{\mathbf{e}}_{(Y)} - (\cos \xi_2 \sin \xi_1 \sin \xi_2/\chi) \hat{\mathbf{e}}_{(Z)}, \end{aligned} \quad (\text{B4})$$

where $\chi := \sqrt{1 - (\sin \xi_1 \sin \xi_2)^2}$.

As anticipated in the main text, it is possible to use such a set of vectors to construct the most general four-velocity that is compatible with the electric-field screening condition. More specifically, the velocity perpendicular to the fields can be written as $\hat{v}_\perp^2 = \mathcal{F}^2(\Omega)(1 - \hat{\mathcal{B}}_{(Y)}^2/\mathcal{B}^2)$. The parallel component, instead, can be parametrized as $\hat{v}_\parallel := q\hat{v}_\parallel^{\text{max}} = q/\hat{\gamma}$ with $q \in (-1, 1)$

and $\hat{\gamma} = \hat{\gamma}_\perp / \sqrt{1 - q^2}$. In the ZAMO Cartesian frame, the components of the spatial velocity read

$$\hat{v}^{(X)} = \left(\mathcal{F} \frac{\hat{\mathcal{B}}^{(Y)}}{\mathcal{B}} + q \sqrt{1 - \mathcal{F}^2 \left(1 - \frac{\hat{\mathcal{B}}^{(Y)2}}{\mathcal{B}^2} \right)} \right) \frac{\hat{\mathcal{B}}^{(X)}}{\mathcal{B}}, \quad (\text{B5})$$

$$\hat{v}^{(Y)} = \mathcal{F} \left(\frac{\hat{\mathcal{B}}^{(Y)}}{\mathcal{B}^2} - 1 \right) + q \sqrt{1 - \mathcal{F}^2 \left(1 - \frac{\hat{\mathcal{B}}^{(Y)2}}{\mathcal{B}^2} \right)} \frac{\hat{\mathcal{B}}^{(Y)}}{\mathcal{B}}, \quad (\text{B6})$$

$$\hat{v}^{(Z)} = \left(\mathcal{F} \frac{\hat{\mathcal{B}}^{(Y)}}{\mathcal{B}} + q \sqrt{1 - \mathcal{F}^2 \left(1 - \frac{\hat{\mathcal{B}}^{(Y)2}}{\mathcal{B}^2} \right)} \right) \frac{\hat{\mathcal{B}}^{(Z)}}{\mathcal{B}}, \quad (\text{B7})$$

where $0 \leq q \leq 1$ is a free coefficients and where the expressions above reduce to the previous results in the literature under the appropriate limits⁶ Furthermore, it is easy to verify that the components (B5) and (B7) satisfy the standard relation $\hat{v}^{(X)} / \hat{\mathcal{B}}^{(X)} = \hat{v}^{(Z)} / \hat{\mathcal{B}}^{(Z)}$.

C. ON THE MAGNETISED TORUS.

Equations (B5)–(B7) show that if the magnetic field is purely toroidal, $\hat{\mathcal{B}} = \hat{\mathcal{B}}^{(Y)} \hat{e}_{(Y)}$, the same is true for the plasma velocity $\hat{v} = q \hat{e}_{(Y)}$, so that the velocity is purely parallel to the field lines. This is the basic dynamical property of the plasma in a Komissarov torus. Furthermore, the condition for the four-velocity to be that of a circular motion with angular velocity Ω_0 as seen by an asymptotic observer requires that $\hat{v}_\parallel = q = \mathcal{F}(\Omega_0)$. We here are interested in tori with a constant specific angular-momentum $\ell_0 := u_\phi / u_t$ and corotating with the BH ($\ell_0 = \text{const.} > 0$), so that the magnetic field is aligned with the azimuthal coordinate, i.e., $\Psi = 0$ and $I < 0$, so that $\xi_{1,2} = \pi/2$ [see Eq. (B3)]. In this case, $\Omega_0 := -(g_{t\phi} + g_{tt}\ell_0) / (g_{\phi\phi} + g_{t\phi}\ell_0)$, and we can express the parallel velocity as a function of ℓ_0 as $\hat{v}_\parallel = \alpha \ell_0 / [\sqrt{\gamma_{\phi\phi}}(\omega_z \ell_0 - 1)]$. With these assumptions, together with the condition $\tilde{v}_{\text{out}} \approx \sqrt{\sigma_0 / (1 + \sigma_0)}$ and $\tilde{\gamma}_{\text{out}} \approx \sqrt{1 + \sigma_0}$ (Liu et al. 2017), Eq. (14) reduces to

$$\varepsilon_\pm^\infty = \alpha \hat{\gamma} \left[\left(1 + \frac{\sqrt{\gamma_{\phi\phi}} \omega_z \hat{v}_\parallel}{\alpha} \right) \sqrt{1 + \sigma_0} \pm \left(\hat{v}_\parallel + \frac{\sqrt{\gamma_{\phi\phi}} \omega_z}{\alpha} \right) \sqrt{\sigma_0} - \frac{1}{4} \frac{\sqrt{1 + \sigma_0} - \hat{v}_\parallel \sqrt{\sigma_0}}{\hat{\gamma}^2 (1 + \sigma_0 - \hat{v}_\parallel^2 \sigma_0)} \right]. \quad (\text{C8})$$

We should note that although we derive Eq. (C8) as a limit of Eq. (14) for $\hat{v}_\parallel = \alpha \ell_0 / [\sqrt{\gamma_{\phi\phi}}(\omega_z \ell_0 - 1)]$ and $\tilde{v}_{\text{out}} \approx \sqrt{\sigma_0 / (1 + \sigma_0)}$, it coincides with Eq. (34) in Comisso & Asenjo (2021), where the plasma was assumed to be in a Keplerian circular orbit in the equatorial plane. Within these limits, therefore, Eq. (34) in Comisso & Asenjo (2021) would provide a multidimensional expression for the plasmoid energies when the Keplerian velocity is replaced by a generic nonplanar one.

We notice that the comoving magnetic field satisfies $b^t = \ell_0 b^\phi$, as typical in the Komissarov torus (Komissarov 2004), with $b^t = -\hat{v}_\parallel \hat{\gamma}_\parallel \hat{\mathcal{B}}^{(Y)} / \alpha^7$. The torus is traditionally defined by equipotential surfaces specified by the condition (Abramowicz et al. 1978; Kozłowski et al. 1978)

$$\mathcal{W} = \frac{1}{2} \ln \left| \frac{\alpha^2 \gamma_{\phi\phi}}{\gamma_{\phi\phi} (1 - \ell_0 \omega_z)^2 - \alpha^2 \ell_0^2} \right| = \text{const.} \quad (\text{C9})$$

We label with $\mathcal{W}_{\text{cusp}}$ the equipotential surface intersecting the equatorial plane at the corresponding cusp radius r_{cusp} , for which the angular momentum matches the Keplerian value $\ell_0 = \ell_K$, and whose value is solely specified in terms of ℓ_0 and a , whereas \mathcal{W}_{in} labels the torus inner edge, that must be specified as a boundary condition. Furthermore, a choice for ℓ_0 uniquely determines the locations of the cusp and of the position of the (pressure) rest-mass density maximum and is constrained to be $\ell_0 > \ell_{\text{ms}}$ (Rezzolla & Zanotti 2013). If $\ell_{\text{ms}} \leq \ell_0 \leq \ell_{\text{mb}}$, then $\mathcal{W}_{\text{cusp}}$ is guaranteed to be non-positive, so that matter and fields can fill the torus up to the cusp, $\mathcal{W}_{\text{in}} \leq \mathcal{W}_{\text{cusp}}$. In the limiting case $\ell_0 = \ell_{\text{mb}}$, the outermost equipotential surface is marginally closed, i.e., $\mathcal{W}_{\text{cusp}} = 0$, while if $\mathcal{W}_{\text{in}} = 0$ the torus is said to be maximally filled. Conversely, if $\ell_0 > \ell_{\text{mb}}$, then $\mathcal{W}_{\text{cusp}} > 0$, and

⁶ For $q = 0$, expressions (B5)–(B7) coincide with (D140) in Chael et al. (2023), and for $q = 1$ with (A12) in Komissarov (2004). Furthermore, the following relations hold: $\hat{\mathcal{B}}^{(X)} = \sqrt{\gamma_{rr}} \hat{\mathcal{B}}^r$, $\hat{\mathcal{B}}^{(Y)} = \sqrt{\gamma_{\phi\phi}} \hat{\mathcal{B}}^\phi$ and $\hat{\mathcal{B}}^{(Z)} = -\sqrt{\gamma_{\theta\theta}} \hat{\mathcal{B}}^\theta$.

⁷ In the notation used in Komissarov (2004), $b^\phi = \pm \sqrt{2p_m / \mathcal{A}}$, where $p_m := b^2 / 2 = \hat{\mathcal{B}}_{(y)}^2 / 2$ and $\mathcal{A} := g_{\phi\phi} + 2\ell_0 g_{t\phi} + \ell_0^2 g_{tt} = \alpha^2 \ell_0^2 (1 - \hat{v}_\parallel^2) / \hat{v}_\parallel^2$.

matter never reaches the cusp being confined within the regions where $\mathcal{W}_{\text{in}} < 0$. In our construction, we always consider tori that are maximally filled, $\mathcal{W}_{\text{in}} = \mathcal{W}_{\text{cusp}} = 0$, since this arguably represents the most interesting configuration, with the torus configuration fully specified by the BH spin and with matter at the cusp prone to accrete onto the BH if perturbed.

The area of the ergobelt is determined by an implicit equation $\mathcal{W}_{\text{in}}(r, \theta) = \mathcal{W}_0$. Because of the non-trivial location of the ergobelt, the surface differential $d\mathcal{A}$ is given by $d\mathcal{A} = \sqrt{\gamma_{\phi\phi}d\phi^2 + \gamma_{\theta\theta}d\theta^2 + \gamma_{rr}dr^2} \Big|_{\mathcal{W}_0}$, with $\phi \in [0, 2\pi]$ and $\theta \in [\theta_*, \pi/2]$, where θ_* is the polar angle that limits the effective region from above at given σ_0 , ℓ_0 and a . The minimum value θ_*^{m} (i.e., the maximum of the integral support, corresponding to the optimal condition $\sigma_0 \gg 1$) can be determined analytically by inverting Eq. (C9) with the supplementary condition $r = r_0(\theta_*^{\text{m}})$, so that

$$\cos(2\theta_*^{\text{m}}) = 1 + \frac{4f_0\ell_0}{a_*M(1-2f_0)} + \frac{4f_0}{a_*^2(1-2f_0)^2} \left(f_0 - 1 + \sqrt{(f_0-1)^2 - a_*^2(1-2f_0)^2 + 2a_*\ell_0f_0(2f_0-1)/M} \right), \quad (\text{C10})$$

where $f_0 := e^{2\mathcal{W}_0}$. For a maximally filled torus, $f_0 = 1$, and $\cos(2\theta_*^{\text{m}}) = 1 - 4\ell_0/a + 4M\sqrt{2\ell_0 - a}/a^{3/2}$, which consistently leads to $\theta_*^{\text{m}} = \pi/2$ for $a_{\text{crit}} = 2(\sqrt{2} - 1)M$.

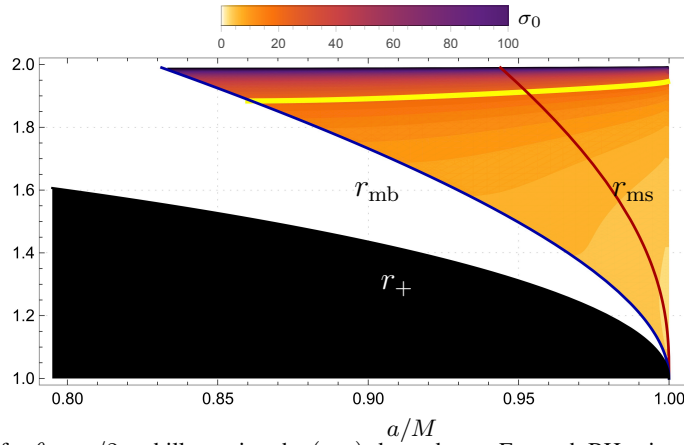


Figure 4. The same as Fig. 2 but for $\theta = \pi/2$ and illustrating the (r, a) -dependence. For each BH spin, the torus cusp is located between r_{mb} (black line) and r_{ms} (red line). Maximally filled tori penetrate the ergosphere ($r_0 = 2M$ on the equator) for $a/M \gtrsim 0.83$. Tori with the cusp at the largest possible position ($r_{\text{cusp}} = r_{\text{ms}}$ or $\ell_0 = \ell_{\text{ms}}$) require larger BH spins, $a/M \gtrsim 0.94$. By increasing the BH spin $r_{\text{ms}} \rightarrow r_{\text{mb}} \rightarrow r_+$, the ergobelt area grows and comparatively smaller magnetisations are needed for a plasmoid-mediated PP.

D. RELATIVISTIC ADIABATIC INCOMPRESSIBLE BALLS (RAIBS).

In what follows we recall the calculation of the energy-at-infinity of a RAIB starting from the energy momentum tensor of an ideal fluid, following the original discussion of Koide and Arai (Koide & Arai 2008). The hydrodynamic energy and angular momentum as measured by a ZAMO can be obtained by projecting the fluid part of the energy-momentum tensor $T_{\text{fl}}^{\mu\nu}$ (i.e., not containing electromagnetic contributions) over the ZAMO tetrad

$$\hat{e}_{\text{fl}} := T_{\text{fl}}^{(T)(T)} = -p + w\hat{\gamma}^2, \quad \hat{\ell}_{\text{fl}} := T_{\text{fl}}^{(T)(Y)} = w\hat{\gamma}^2\hat{v}^{(Y)}, \quad (\text{D11})$$

where $T_{\text{fl}}^{\mu\nu} := wu^\mu u^\nu + pg^{\mu\nu}$, with w and p the enthalpy density and the pressure measured in the comoving frame of the fluid, and $\hat{\gamma}$ the Lorentz factor of the fluid with respect to the ZAMO. The conserved Noether currents in stationary and axisymmetric hydrodynamic flows, $\mathcal{J}_E^\mu = -T^\mu{}_\nu(\partial_t)^\nu$ and $\mathcal{J}_L^\mu = T^\mu{}_\nu(\partial_\phi)^\nu$, can be expressed as combinations of quantities measured in the ZAMO frame, with their redshifted temporal components being respectively the energy density and angular-momentum-at-infinity, respectively $e^\infty = \alpha\hat{e} + \sqrt{\gamma_{\phi\phi}}\omega_z\hat{\ell}$, and $\ell^\infty = \sqrt{\gamma_{\phi\phi}}\hat{\ell}$.

Assuming the fluid to be perfect and described by an ideal-fluid equation of state, the pressure can be expressed as $p = \rho\epsilon(\Gamma - 1)$, with Γ the adiabatic index, ρ the rest-mass density, and ϵ the specific internal energy. As a result, the enthalpy density is $w = \rho(1 + \epsilon\Gamma) = \rho + 4p$ for a completely degenerate relativistic fluid with $\Gamma = 4/3$ (Rezzolla & Zanotti 2013). For simplicity, we assume that the rest-mass density of the plasmoid is much smaller than the internal energy density, i.e., $\rho \ll \rho\epsilon$, so that the enthalpy density can be approximated as $w = \rho + 4p \approx 4p$. Future improvement to the approach followed here (and in the

literature) will concentrate on better estimating not only the role of the rest-mass density over the internal energy density, but also on the role played by the magnetisation in the plasma.

Bearing these considerations in mind, we recall that the RAIB model assumes that the rest-mass density is localised, so that, in the ZAMO frame, $\rho = m\delta^3(\hat{\mathbf{x}} - \hat{\mathbf{x}}(t))/\hat{\gamma}(t)$, where m is the rest-mass of the RAIB. This allows to easily integrate the energy and angular momentum density over the entire three-space in the ZAMO frame to obtain the total energy and angular-momentum-at-infinity associated to a RAIB

$$E_{\text{RAIB}}^\infty = \alpha \left[H\hat{\gamma} \left(1 + \frac{\sqrt{\gamma_{\phi\phi}}}{\alpha} \omega_z \hat{v}^{(Y)} \right) - \frac{U(\Gamma - 1)}{\hat{\gamma}} \right], \quad L_{\text{RAIB}}^\infty = \sqrt{\gamma_{\phi\phi}} H\hat{\gamma} \hat{v}^{(Y)}. \quad (\text{D12})$$

In obtaining the expressions above we have written the total enthalpy as $H = m(1 + \epsilon\Gamma)$ and the total internal energy as $U = m\epsilon$ [Eq. (D12) coincides with Eq. (14) in the main text].

We conclude this section by clarifying an inconsistency often encountered in the literature that adopts the RAIB prescription. It should be noted that in [Comisso & Asenjo \(2021\)](#) [see Eq. (25) therein], and in many related works, the expression above is improperly identified as an energy density. The inconsistency becomes evident once realised that if Eq. (25) in [Comisso & Asenjo \(2021\)](#) corresponds to an energy density, it can be further integrated in space to obtain the total energy, and upon taking the point-like particle limit (i.e., $U = 0$ and $H = m$) in flat spacetime ($\alpha = 1$ and $\omega_z = 0$), this would lead to $E = m$. Conversely, the point-like particle limit in flat spacetime of Eq. (14) leads to the correct result for the total relativistic energy of a single particle, i.e., $E = m\hat{\gamma}$.

DATA AVAILABILITY

All data are incorporated into the article and its online Supporting Information.